

# A way to deal with the fringe-like pattern in VIMOS-IFU data <sup>★</sup> (Research Note)

C. Lagerholm<sup>1</sup>, H. Kuntschner<sup>1</sup>, M. Cappellari<sup>2</sup>, D. Krajnović<sup>1</sup>, R. M. McDermid<sup>3</sup>, and M. Rejkuba<sup>1</sup>

<sup>1</sup> European Southern Observatory, Karl-Schwarzschild-Str 2, 85748 Garching bei München, Germany  
e-mail: clagerho@eso.org

<sup>2</sup> Sub-department of Astrophysics, University of Oxford, Denys Wilkinson Building, Keble Road, Oxford OX1 3RH

<sup>3</sup> Gemini Observatory, Northern Operations Center, 670 N. A'ohoku Place, Hilo, HI 96720, USA

Received 31 January 2012 / Accepted 12 Mars 2012

## ABSTRACT

**Context.** The use of integral field units (IFUs) is now commonplace at all major observatories offering efficient means of obtaining spectral as well as imaging information at the same time. IFU instrument designs are complex and spectral images have typically highly condensed formats, therefore presenting challenges for the IFU data reduction pipelines. In the case of the VLT VIMOS-IFU, a fringe-like pattern affecting the spectra well into the optical and blue wavelength regime as well as artificial intensity variations, require additional reduction steps beyond standard pipeline processing.

**Aims.** In this research note we propose an empirical method for the removal of the fringe-like pattern in the spectral domain and the intensity variations in the imaging domain. We also demonstrate the potential consequences for data analysis if the effects are not corrected. Here we use the example of deriving stellar velocity, velocity dispersion and absorption line-strength maps for early-type galaxies.

**Methods.** We derive for each spectrum, reduced by the ESO standard VIMOS pipeline, a correction-spectrum by using the median of the eight surrounding spectra as a proxy for the unaffected, underlying spectrum. This method relies on the fact that our science targets (nearby early-type galaxies) cover the complete field-of-view of the VIMOS-IFU with slowly varying spectral properties and that the exact shape of the fringe-like pattern is nearly independent and highly variable between neighboring spatial positions. Quadrant-to-quadrant intensity variations are corrected for in an independent step.

**Results.** We find that the proposed correction methods for the removal of the fringe-like pattern and the intensity variations in VIMOS-IFU data-cubes are suitable to allow for meaningful data analysis in our sample of nearby early-type galaxies. Since the method relies on the scientific target properties it is not suitable for general implementation in the pipeline software for VIMOS.

**Conclusions.**

**Key words.** Methods: data analysis – Galaxies: abundances – Galaxies: kinematics and dynamics

## 1. Introduction

Integral field units (IFU), combining spectrographic and imaging capabilities, are used to obtain spatially resolved spectra over a typically contiguous field-of-view (FoV). These instruments, offering an enormous gain in observing efficiency compared to classical long-slit spectrographs, are now used at all major observatories (e.g. GMOS at Gemini, SAURON at WHT and OSIRIS at Keck). The often complex instrument designs and the dense information content on the detectors lead to challenges for the data-reduction. At the VLT, the Visible Multi-Object Spectrograph (VIMOS) features an IFU containing 6400 microlenses coupled to fibres and covering wavelengths between 4000 – 10150 Å with a set of six grisms (Le Fèvre et al. 2003). With the medium and high-resolution grisms (R=580-2500), the spectra of a single pseudo-slit will cover the entire length of the CCD; therefore, only one pseudo-slit can be used. The IFU head will then be partially masked by a shutter, so that only a square of 40 x 40 fibres is used yielding, either a FoV of 27'' x 27'' at 0'.67 per fibre, or a FoV of 13'' x 13'' at 0'.33 per fibre. The light is fed to four independent spectrographs each covering a quarter of the FoV and recording spectra on its own

CCD. The four identical channels of VIMOS are referred to as quadrants. The VIMOS data reduction pipeline (Izzo et al. 2004; Zanichelli et al. 2005) removes the instrumental signature from the spectra of each quadrant and combines data into a single data cube covering the full FoV.

It has been known for several years (e.g. Jullo et al. 2008, VLT VIMOS manual<sup>1</sup>) that spectra of the VIMOS-IFU in conjunction with the “HR-Blue” and “HR-Orange” grisms exhibit spectral features visually similar to fringes. Normally, fringes arise from the interference in the CCD detection layer, between incident light and the light reflected from interfaces of the CCD layers. Given the typical thickness of this layer, fringes are observed at red wavelengths (>7000 Å). Yet, in the case of the VIMOS-IFU, the features (see Fig. 1) which resemble fringes, are present over the whole wavelength range, suggesting that they are caused by a different mechanism. For the rest of this research note we will call these features “fringe-like patterns”.

Jullo et al. (2008) carried out an investigation into the possible origin of the fringe-like pattern. They concluded that it either originates from inside the mask at the pseudo-slit level or from the not perfect position of the masks themselves. However, due

<sup>★</sup> Based on observations taken at the La Silla Paranal observatory withing Program ID: 079.B-0402

<sup>1</sup> [http://www.eso.org/sci/facilities/paranal/instruments/vimos/doc; issue 88.0, Sect. 2.8.1](http://www.eso.org/sci/facilities/paranal/instruments/vimos/doc;issue 88.0, Sect. 2.8.1)

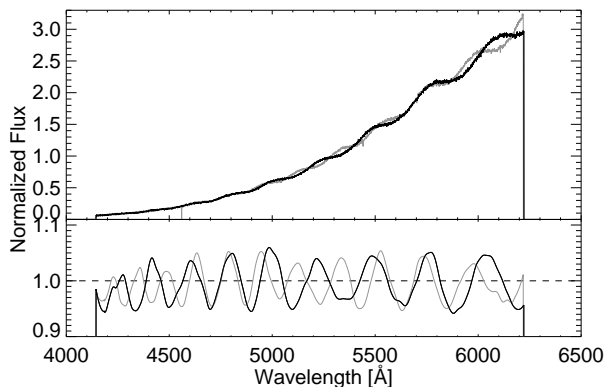


**Fig. 1.** The fringe-like pattern in the VIMOS-IFU used with the “HR-Blue” grism. Top panel: Flat-field spectrum from a single spatial element (fibre) clearly showing the effects of the fringe-like pattern (black). Bottom panel: the corresponding, normalized correction function for this fibre (black). In grey we show the flat-field spectrum and correction function from the same spatial element but observed in a different night.

to the fact that the fringe-like pattern varies between exposures they proposed that the effect probably arises from flexure of the prisms in the pseudo-slit. Most likely the cause of the fringe-like pattern in the spectra is the presence of a “pseudo etalon”, of approximately 5-10 micron thickness, associated with the fibre output prism (H. Dekker, private communication).

In this research note we present an empirical method for removing the fringe-like pattern which is implemented as an additional step in the data reduction before stacking individual exposures. We first noted the fringe-like pattern during the analysis of our own VIMOS-IFU observations of nearby Early-Type Galaxies (ETG) utilizing the “HR-Blue” grism (wavelength range 4150-6200 Å) with a  $27'' \times 27''$  FoV.

It is for this instrument mode and specific targets that we have constructed and tested the method to remove the fringe-like pattern. Typical for nearby ETGs, our targets show a very smooth surface brightness profile and cover the whole FoV of the VIMOS-IFU. The full scientific investigation of these ETGs will be presented in a future paper (Lagerholm et al. in prep.). Here we only show results for the galaxy NGC 3923 which are used to explain the correction method.

The paper is organized as follows. Sec. 2 describes the challenges arising from the data reduction process. In Sec. 3 our method used for correcting the intensity differences and fringe-like pattern is described. In Sec. 4 we describe the impact of the corrections on the scientific analysis and provide a map of the typical strength of the fringe-like pattern for the VIMOS-IFU. Finally, in Sec. 5 we present our conclusions.

## 2. Challenges of the Data Reduction

The data reduction was mainly performed with the ESO pipeline (version 2.3.3) using the standard settings described in the pipeline manual<sup>2</sup>. The pipeline processing steps included the subtraction of the median combined bias image, creation of the spectral extraction mask from a flat field image taken immediately following the science exposure, and wavelength calibration constructed from the HeArNe lamp exposures. The flux calibra-

tion, which is normally performed within the pipeline, did not deliver satisfactory results for some standard stars. Therefore, we opted to perform the flux calibration outside the pipeline with IRAF using the `standard`, `sensfunc` and `calibrate` tasks. This also gives us the possibility to combine several standard stars for the flux calibration, which is not possible within the ESO pipeline. The standard stars used for the flux calibration are extracted using the pipeline, where the spectrum is derived by addition of several spatial elements thus diminishing the signatures from the fringe-like pattern. The final flux calibration curve, which is derived separately for each quadrant, was constructed by fitting a third order polynomial to the standard star data. The low order polynomial fit ensures that any signatures of the fringe-like pattern are removed.

In the following we describe three data reduction issues which remain after the standard pipeline procedure: (1) intensity differences between quadrants, (2) intensity stripes across the complete FoV and (3) the fringe-like pattern in the spectral domain. All three effects, if not accounted for, can significantly affect the scientific analysis, specifically when the continuum shape and/or the continuum level play a role.

### 2.1. Quadrant-to-quadrant throughput variations

Due to the four independent spectrographs used in VIMOS (Le Fèvre et al. 2003), each re-constructed data-cube is composed of four quadrants (Q1 to Q4; see also Fig. 2). After a standard pipeline reduction, the quadrants typically show different intensity levels as shown in the top left panel of Fig. 2. These differences (accounting for up to 40% in our data sample) give rise to sharp drops/increases in intensity along the connecting quadrant edges. Although these throughput differences between quadrants do not affect the extraction of e.g. kinematics and line-strengths measurements for individual spectra, a correction is needed when a reconstructed image is analyzed or when regions across the quadrant edges are binned up to reach a specific S/N requirement.

### 2.2. Intensity stripes

In addition to the quadrant-to-quadrant intensity variations, the reconstructed images from the VIMOS-IFU cubes show diagonal intensity stripes across the FoV (Fig. 2; top left panel). The intensity variations in these diagonal stripes reach up to  $\sim 15\%$  in our data. When comparing individual spectra located on the peak of a given stripe with the ones next to it, the spectra associated with the stripe show an overall higher flux level over the whole wavelength range. If these stripes were to be caused by the instrument, one would expect discontinuities at the quadrant borders since the four quadrants originate from independent spectrographs. The fact, that the stripes seem to propagate right through quadrant borders points towards a pipeline reduction problem. The underlying cause is presently unknown.

### 2.3. Fringe-like patterns

More than half of the spectra in a VIMOS data-cube are significantly affected by the fringe-like pattern (see Fig. 1). The amplitude and the frequency of the pattern is not randomly distributed between fibres but shows a clear connection to individual fibre modules. Important to note is that the fringe-like pattern is also present in the raw data, thus not an artifact created by the extraction process of the spectra. The fringe pattern shifts monoton-

<sup>2</sup> <http://www.eso.org/sci/software/pipelines/>

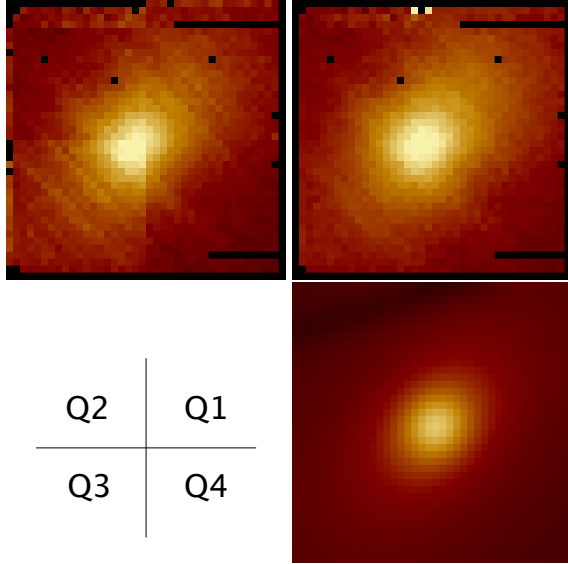


**Fig. 2.** Top panels: Reconstructed images derived from a VIMOS-IFU data cube showing the central  $26''.8 \times 26''.8$  of the early-type galaxy NGC 3923. Top left: an example of the image derived from the original data cube as produced by the pipeline; Top right: image derived from the corrected cube. Bottom left: Numbering scheme of the four VIMOS-IFU quadrants; Bottom right: For comparison we show an ACS/WFC F606W image of NGC 3923, binned up to the spatial sampling, field-of-view and broadened to  $\sim 1''.2$  seeing of the VIMOS data-cube. For the three images of NGC 3923 the orientation is north to the right and east to the top.

ically inside a given module but strong breaks appear between fibre modules as illustrated in Fig. 3. In quadrant Q2 almost all spectra are affected while the other quadrants also show fibre modules with negligible or no fringe-like pattern. For each fibre the fringe-like pattern resembles to first order the transmittance function of an etalon with a reflectance of order 1 – 3% and a thickness of order 3 – 10  $\mu\text{m}$  (see Fig. 4 for examples). However, the variation of the amplitude with wavelength and deviations from a simple etalon transmission function suggest that more than one layer and complex reflectance variations with wavelength may be present in reality.

An important point to note is that the fringe pattern is not stable with time (see Fig. 1; grey lines). Even flat fields taken during the night and adjacent to the science exposure typically do not show the same fringe-like pattern as in the science data. This can be explained by the change of instrument rotator angle and associated flexure in the instrument. During the science exposure the rotator angle of the instrument changes in order to follow the target, causing a different bending of the fibres and therefore a variation of the flexure of the prisms in the pseudoslit and the fringe-like pattern. The flat-field taken at the end of the science exposure only reflects the pattern at the final rotator angle. Due to hysteresis effects, returning to the same rotator angle also leads to a changed fringe-like pattern (Jullo et al. 2008).

We further note, that the observed fringe-like pattern has a frequency and amplitude similar to stellar absorption features in our target galaxy spectra and thus simple filtering with Fourier techniques is not suitable for removing the effect. For the most affected spectra the pattern accounts for  $\sim 13\%$  difference in intensity, peak-to-valley (hereafter PTV; see also Sec. 4.3).

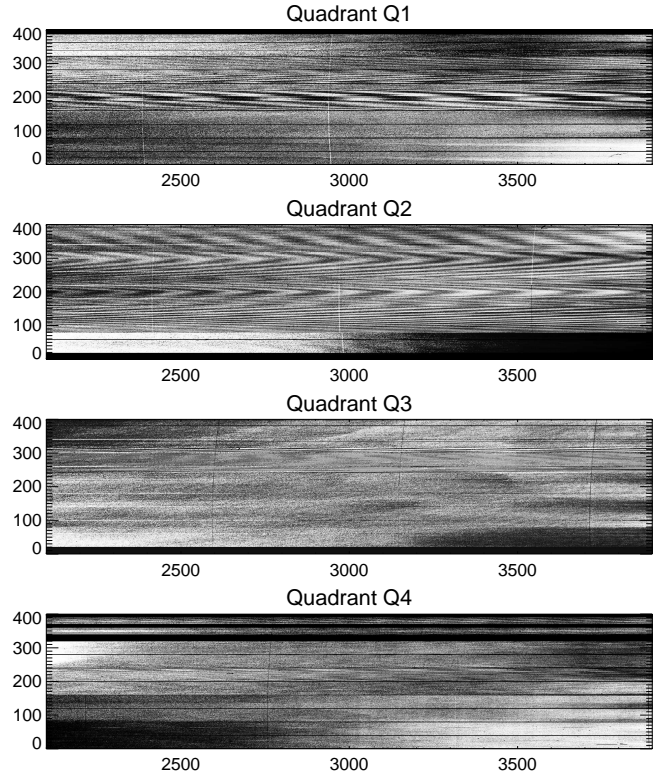


**Fig. 3.** Variation of the fringe-like pattern for extracted flat-field spectra where the median lamp spectrum has been removed. Each row represents one fibre and wavelength increases from left to right. A subset of the wavelength range, covering pixels 2100 to 3900 and thus corresponding to about 5130 to 5675  $\text{\AA}$ , is shown. The example spectrum shown in Fig. 1 is taken from quadrant Q3 where only one fibre module shows a significant fringe-like pattern.

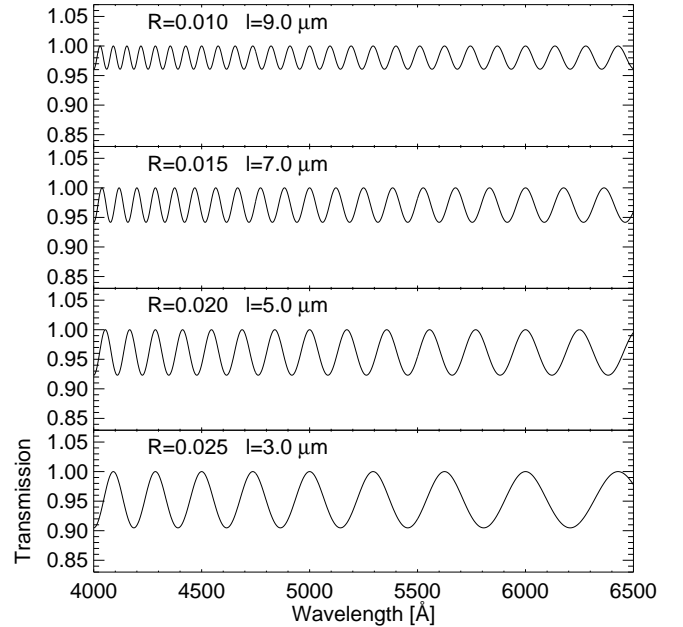


**Fig. 4.** The transmission of an etalon as a function of wavelength for a few values of reflectance  $R$  and etalon thickness  $l$ . The values are indicated inside each panel.

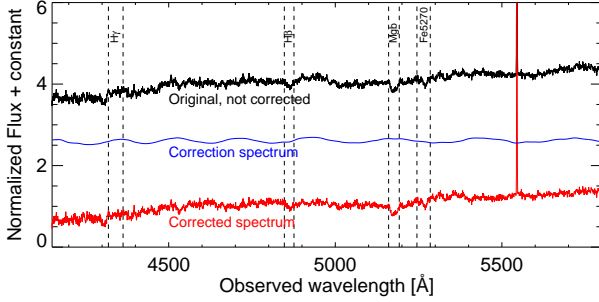


**Fig. 5.** Example of the correction made for each individual spectrum. Here one of the most affected spectra for the galaxy NGC 3923 (not sky-subtracted) is shown. The top black spectrum represent the original spectrum at one spatial position. The middle blue spectrum shows the correction spectrum derived with our method. The bottom red spectrum shows the corrected spectrum. The black dashed vertical lines indicate the central bandpasses of the line-strength indices  $H\gamma$ ,  $H\beta$ ,  $Mg\ b$  and  $Fe5270$ .

### 3. The correction method

After the extraction and wavelength calibration of spectra using the VIMOS pipeline and flux calibration within IRAF, we correct for the quadrant-to-quadrant intensity differences. We assume that the intensity correction is constant with wavelength and uniform within each quadrant, and re-normalize quadrants Q1, Q3 and Q4 to quadrant Q2 (see Fig. 2; top right panel). The re-normalization is done by comparing the intensity levels of the neighbouring pixels at the quadrant borders and taking a first order gradient in intensity across the borders into account.

Now we can turn our attention to the fringe-like pattern in the spectra and the intensity stripes seen in the reconstructed image. For both, the correction of the fringe-like pattern and the intensity-stripes, the underlying main assumption is that, to first order, the effects are localized, i.e. they are independent between even neighbouring spectra. This is a reasonable assumption if the effects are caused by a non-perfect fixation of the fibre to the prism (Jullo et al. 2008) creating a “pseudo etalon” associated with the fibre output prism.

For each spectrum in the data-cube we calculate the *median* spectrum from the nearest eight spatially surrounding spectra. This median spectrum is, if all eight spectra have different fringe-like patterns, to first order unaffected by the pattern. Due to the fact, that for our targets the spectral properties are changing relatively slowly as function of spatial position and that the signal in the neighbouring spectra is correlated due to natural seeing effects, this median spectrum can be used as an approximation of the underlying, “true” spectrum in the central pixel. The ratio of the median spectrum and that of the central pixel will provide an estimate of the fringe-like pattern, i.e. a correction spectrum which by construction has a mean  $\sim 1$ . Due to the typically limited S/N in the correction spectrum we decided to smooth the correction spectrum within IDL using the *lowess* function, which is part of The IDL Astronomy User’s Library (Landsman 1993). We applied a smoothing function using a second order polynomial for each step of 150 pixels in our case. The resulting correction spectrum preserves the overall shape and amplitude of the fringe-like pattern with negligible noise at smaller wavelength scales (see Fig. 5).

The fringe-like pattern is then removed from the original data-cube by dividing each spectrum with the corresponding smoothed correction spectrum. This procedure is done for all the spectra in the cube, except for the outermost corner spectra and spectra in the neighborhood of regions with dead fibres (shown as black dots or black stripes in the reconstructed IFU image in Fig. 2). Spectra, for which we could not derive a correction spectrum based on the median of at least five or more surrounding spectra were set to zero.

A drawback of the above described procedure is the effective smoothing which is applied over the scale length of roughly three spatial elements. Particularly, in the centre of the target galaxies this is a non-desirable effect which has to be accounted for in any subsequent analysis. However, the question arises if the median of the eight surrounding spectra is providing a good enough estimate of the underlying spectrum or if one would need to combine even more spectra to obtain a meaningful correction spectrum.

In order to test the effect of increasing the number of spatial elements used to derive the median spectrum we re-constructed a data-cube for an internal flat-field exposure. Here it can be safely assumed that over the scale length of several pixels the underlying, uncontaminated spectrum does not change. In our test we doubled the number of spectra used for the median spectrum, using both the eight surrounding spectra plus eight spectra, equally spaced, from the next closest ring of spectra in the data cube.

Fig. 6 shows the maximum difference between the correction spectrum constructed from eight and 16 neighboring spectra for the whole VIMOS-IFU FoV. Except for a few outliers, especially in the top of quadrant Q2, which show differences up to 5%, most of the correction spectra show difference of less than 0.6%. We conclude that the median of eight spectra is already sufficient to produce a correction spectrum with an accuracy of about 0.6%. Given that our typical corrections are of order 6% and that we are going to combine several exposures to form the final data cube for analysis, this accuracy appears sufficient. Furthermore, visual inspection of the differences between taking the median of eight or 16 spectra indicates that the central wavelength range, containing the most important absorption features, is well behaved while the extreme differences are often found at the edges of the wavelength range.

## 4. Results

In this section we first describe the potential consequences of an imperfect data reduction (Sec. 3) for a typical kinematics and stellar population analysis of early-type galaxies. We then demonstrate in Sec. 4.2, by using the example of VIMOS-IFU observations of the ETG NGC 3923, to which extent the proposed correction method removes the effects. Finally, we provide a map of the VIMOS-IFU FoV showing the regions which are most affected by the the fringe-like pattern (see Sec. 4.3).

### 4.1. Science impact

Both the intensity differences and the fringe-like pattern, if not corrected for, will affect the science derived from the data. When looking at the whole spectral range (see Fig. 5) it can be hard to see the effects that the corrections have on the spectra. In Fig. 7 we have therefore zoomed into the spectral range of two absorption features,  $H\gamma$  and  $Mg\ b$ , used for the line-strength analysis of the stellar populations in NGC 3923. In the Lick/IDS system (Trager et al. 1998), absorption line strengths are measured by



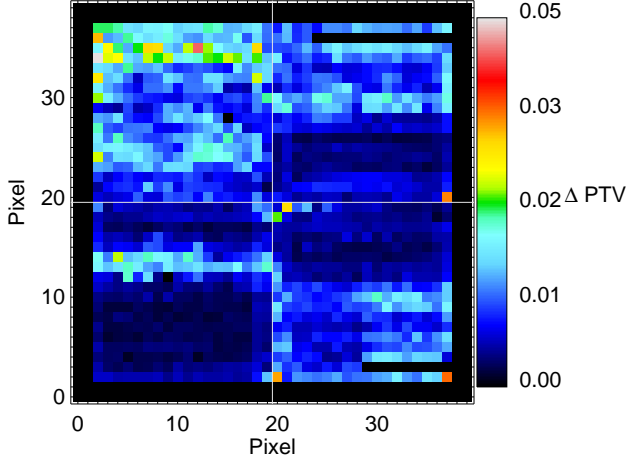


**Fig. 6.** The maximum differences between the fringe-like patterns, created from using eight surrounding spectra and 16 surrounding spectra, in the wavelength range 5188 – 5620 Å. The white solid lines indicate the borders of the different quadrants. The quadrants are positioned as shown in Fig. 2 bottom left panel.

indices, where a central feature bandpass is flanked to the blue and red by pseudo-continuum bandpasses (see Fig. 7). The mean level of the two pseudo-continuum regions is determined independently on each side of the feature bandpass and a straight line is drawn through the midpoint of each one. The difference in flux between this line and the observed spectrum within the feature bandpass determines the index. In our example, shown in Fig. 7, it is clearly demonstrated that the fringe-like pattern correction changes the continuum level of the spectra on a scale relevant for the determination of the line-strength. Particularly, the pseudo-continuum level, used for the line-strength analysis, will be located wrongly. For the example spectrum shown in Fig. 5, the Mg *b* and H $\gamma_A$  indices change by  $-0.08$  and  $-0.28$  Å, respectively (not corrected – corrected spectrum).

The example shown in Fig. 7 represents only one realization of the fringe-like pattern and it can be easily seen how different patterns could lead to a whole range of changes to the line-strength measurements (positive and negative changes). Furthermore, velocity and velocity dispersion measurements will also be affected to some extent. However, here the effects are somewhat smoothed out since the measurements are typically obtained from a wavelength range covering several wiggles/periods of the fringe-like pattern.

In order to evaluate the effects more quantitatively, we set up simple simulations. The fringe-like pattern is not a simple sinusoidal function, however, we approximate it with a sinusoidal with the mean frequency of the fringe-like pattern and varying phase and amplitude covering the full range seen in the real data. This sinusoidal is multiplied to a fringe-free galaxy spectrum (a galaxy spectrum already corrected for the fringe-like pattern) to simulate the effects of the fringe-like pattern. In our simulations we changed the amplitude (PTV between 0 and 15%) and phase (between 0 and  $2\pi$ ) of the sinusoidal each in seven steps and measured for each spectrum the velocity, velocity dispersion and line-strengths. The results are summarized in Fig. 8. As expected, the exact location of the fringe-like pattern determines if a given quantity is changed in a positive or negative direction. Even for large amplitudes, a negligible change is possible when

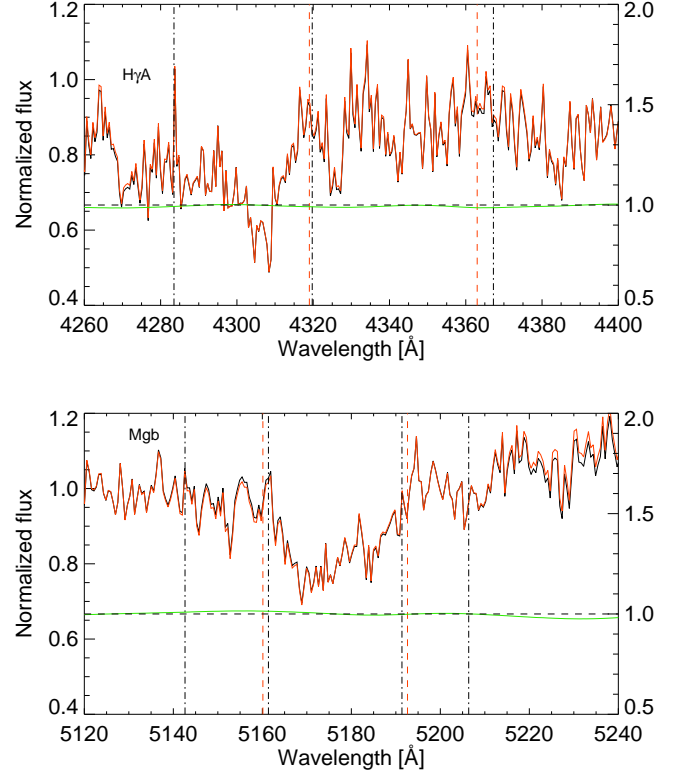


**Fig. 7.** Difference between a spectrum corrected for the fringe-like pattern (red solid line) and a spectrum which was not corrected (black solid line). The green solid line shows the correction function across the wavelength range where the scaling is given at the right y-axis. The line strength is measured between the red dashed lines and the continuum band-passes between the dashed-dotted vertical lines. The line strengths measurements for these two lines in the non-corrected and corrected spectrum are for H $\gamma_A = -4.79 \pm 0.33$  Å, and  $-5.07 \pm 0.37$  Å, and for Mg *b* =  $5.33 \pm 0.28$  Å, and  $5.25 \pm 0.32$  Å, respectively.

the effects of the fringe-like pattern cancel out. However, the exact phase for this configuration is dependent on the quantity under consideration.

For a typical amplitude of 5% (PTV = 0.10) the velocities can be affected by up to  $\pm 20$  km s $^{-1}$ , the velocity dispersion up to  $\pm 40$  km s $^{-1}$ , the Mg *b* index by up to  $\pm 0.5$  Å, the H $\gamma_A$  index up to  $\pm 1$  Å and the Fe5270 index up to  $\pm 0.3$  Å.

Overall, we conclude that for these typical correction spectrum amplitudes (see also Sec. 4.3), the fringe-like pattern can have a severe influence on the scientific analysis; especially for kinematical and line-strength measurements. We emphasize that the above numbers are only valid for an individual exposure and that the combination of several exposures or fibres will significantly mitigate the problem.

#### 4.2. Application to our data

Overall, our correction method offers significant improvements compared to the results obtained from uncorrected data. In the reconstructed image the intensity differences, both between quadrants and between individual spectra seen as stripes, are now considerably smaller (on average  $< 5\%$ ; see Fig. 2; top left panel). The overall morphology of the science target (e.g. the

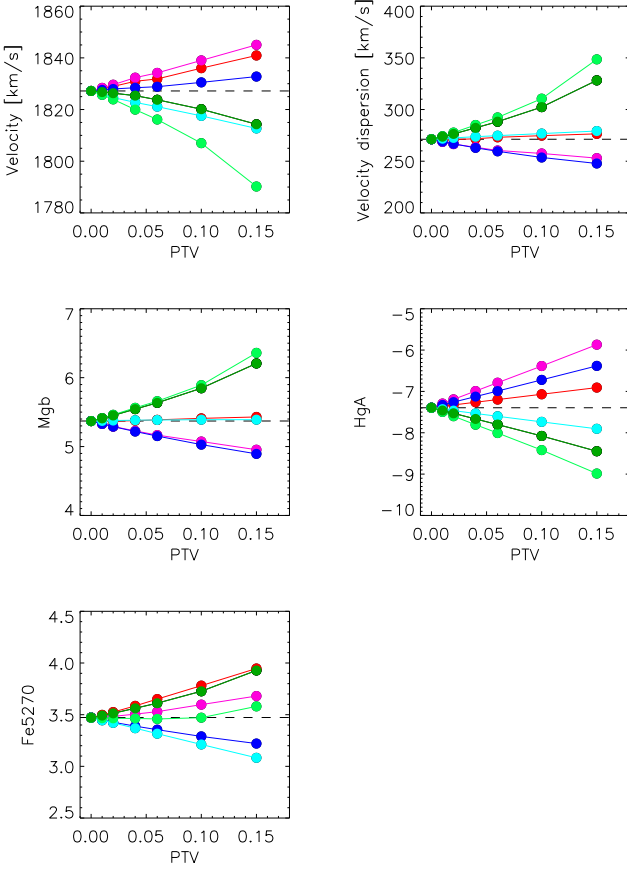


**Fig. 8.** Changes in velocity, velocity dispersion and the line strengths,  $Mg\ b$ ,  $H\gamma_A$  and  $Fe5270$  depending on the PTV of the fringe-like pattern (sinusoidal). Different colors indicates different phase shifts of the sinusoidal, equally separated between 0 and  $2\pi$ . The shift in color goes from dark green, red, magenta, blue, light blue, light green, back to dark green. The black dashed lines indicates the correct values given by the fringe free galaxy spectrum.

isophotes) is now in much better agreement with a direct image although it does not reach its level of quality (see Fig. 2; bottom right panel).

However, the most important part of the correction is the removal of the fringe-like pattern from the spectra. In Fig. 9 we show the line strengths maps for the  $Mg\ b$ ,  $H\gamma_A$  and  $Fe5270$  indices of NGC 3923, for both the fringe-like pattern corrected cube and the uncorrected cube. Each cube is the combination of five individual exposures. In the case of the corrected cube each individual exposure was corrected before combination.

The overall improvement in quality can be directly seen by comparing the non-corrected and corrected line strength maps in Fig. 9. The maps constructed with the corrected cubes have metal index values ( $Mg\ b$  and  $Fe5270$ ), which peak towards the centre, while the maps for the non-corrected cubes show a more scattered morphology and are not as smooth as expected for an ETG (e.g. Kuntschner et al. 2006). However, the expected differences between the corrected and non-corrected line-strength maps are not as large as one would expect from our simulations described in Sec. 4.1. This can be understood when considering that the final cube was built from the combination of five

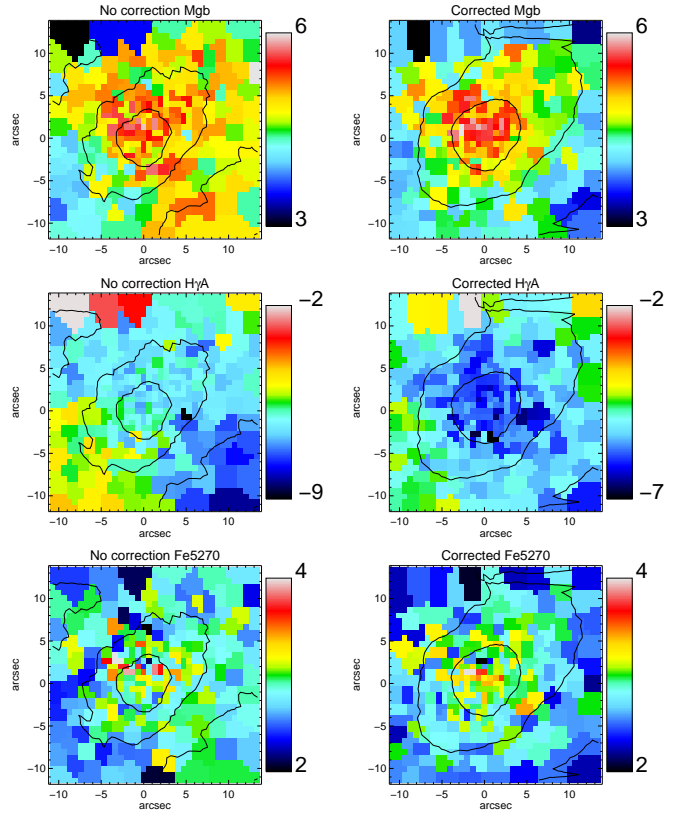


**Fig. 9.** Line strengths maps for NGC 3923 over  $Mg\ b$ ,  $H\gamma_A$  and  $Fe5270$ . In the three plots to the left the cubes are not corrected and in the three plots to the right the cubes are corrected for the fringe-like patterns. The spectra used for the line-strengths analysis are binned, using Voronoi Binning (Cappellari & Copin 2003), in order to have at least a S/N of 60. The velocities and velocity dispersions are calculated using pPFX (Cappellari & Emsellem 2004) and are used in the line-strength measurements. The line strengths are measured using the same principle as in Kuntschner et al. (2006).

exposures which helped to average out some of the fringe-like pattern.

The effects of the fringe-like pattern scale with the signal in the data since it is a multiplicative effect. Therefore, a low signal-to-noise exposure, e.g. a sky exposure, will not display a prominent fringe-like pattern. The fringe-like pattern will be hidden in the noise, and we are not able to correct them using our proposed method. However, for the sky subtraction of the galaxies we use a median over the whole sky cube, thus the sky spectrum will essentially be free from the fringe-like pattern.

For science targets for which our proposed method is not suitable (e.g. low signal-to-noise or highly variable spectral properties across the FoV) one can reduce the fringe-like pattern by averaging several, slightly dithered, exposures. The appropriate number of exposures surely depends on the science goals and the target itself, but as a guideline we would recommend to obtain on the order of eight exposures thereby mimicking the averaging effect of our proposed method.

#### 4.3. Spatial map of the fringe-like pattern effect

The four quadrants are not all equally affected by the fringe-like pattern – there are variations both between the quadrants and

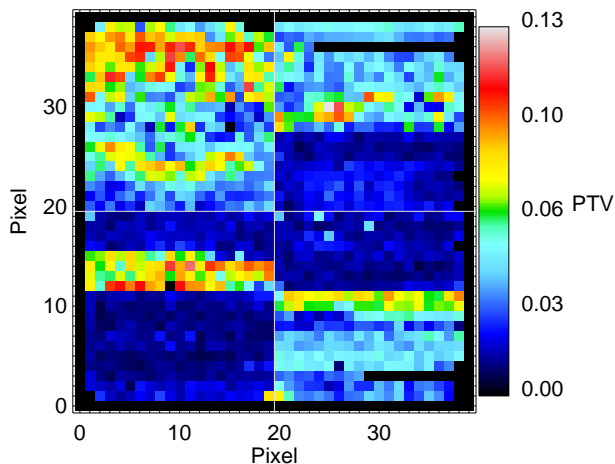


**Fig. 10.** Spatial map of the maximum variations (PTV) in the correction spectra as derived from a flat-field and in the wavelength range 5188 – 5620 Å. Regions with a strong fringe-like pattern are clearly visible and connected to certain fibre models (see also Fig. 3). The white solid lines indicate the borders of the quadrants. The quadrants are positioned as shown in Fig. 2, bottom left panel.

within the quadrants. Fig. 10 shows the maximum PTV values per spatial element, derived from the correction spectra of a flat field. Regions with a prominent fringe-like pattern, connected to individual fibre modules (see also Fig. 3) are clearly visible. While the precise phase and amplitude of the fringe-like pattern varies between exposures, the spatial regions which are significantly affected in a VIMOS-IFU cube can be well characterized. For example, quadrant Q2 is the most affected quadrant. The other three quadrants feature regions which are much less or not at all affected. The maximum PTV values in a cube reach 0.13 while the mean value for the affected fibre models is about 0.06, i.e. an amplitude of 3%.

## 5. Conclusions

In this research note we have shown that additional data reduction steps, beyond the standard ESO data reduction pipeline recipes, can improve the quality of the reduced spectra and therefore the science analysis of VIMOS-IFU data obtained with the “HR-Blue” grism. The correction of quadrant-to-quadrant intensity variations and intensity stripes leads to significantly improved reconstructed images. More than half of the VIMOS-IFU spectra obtained with the “HR-Blue” grism show, across the full wavelength range, spectral features visually similar to fringes. Unfortunately, the fringe-like pattern is not stable in time and can therefore not be removed in the flat-fielding process. Our proposed empirical method of minimizing the effects of the fringe-like pattern enables a meaningful kinematics and line-strength analysis for nearby early-type galaxies as demonstrated for the case of NGC 3923. The combination of several exposures into a combined cube also mitigates the fringe-like pattern, however, our newly proposed method working on individual exposures before combination, provides better results. We note, that the proposed correction method is only tested for and will work with objects similar to our science targets (nearby early-type galaxies) which cover the whole VIMOS-IFU FoV and display slowly varying spectral properties over the FoV. When dealing with ob-

servations that have strongly varying background or low intensities preferably a different approach should be adopted. In these cases it may be better to rely on the combination of several individual exposures to reduce the effects of the fringe-like pattern or to aim for a full modeling of the fringe-like pattern.

*Acknowledgements.* We would like to thank H. Dekker for useful comments on the possible origin of the fringe-like pattern. We thank the anonymous referee for useful comments. MC acknowledges support from a Royal Society University Research Fellowship. RMcD is supported by the Gemini Observatory, which is operated by the Association of Universities for Research in Astronomy, Inc., on behalf of the international Gemini partnership of Argentina, Australia, Brazil, Canada, Chile, the United Kingdom, and the United States of America.

## References

- Cappellari, M. & Copin, Y. 2003, MNRAS, 342, 345
- Cappellari, M. & Emsellem, E. 2004, PASP, 116, 138
- Izzo, C., Kornweibel, N., McKay, D., et al. 2004, The Messenger, 117, 33
- Jullo, E., Christensen, L., Smette, A., et al. 2008, in 2007 ESO Instrument Calibration Workshop, ed. A. Kaufer & F. Kerber, 343–346
- Kuntschner, H., Emsellem, E., Bacon, R., et al. 2006, MNRAS, 369, 497
- Landsman, W. B. 1993, in Astronomical Society of the Pacific Conference Series, Vol. 52, Astronomical Data Analysis Software and Systems II, ed. R. J. Hanisch, R. J. V. Brissenden, & J. Barnes, 246
- Le Fèvre, O., Saisse, M., Mancini, D., et al. 2003, in Society of Photo-Optical Instrumentation Engineers (SPIE) Conference Series, Vol. 4841, Society of Photo-Optical Instrumentation Engineers (SPIE) Conference Series, ed. M. Iye & A. F. M. Moorwood, 1670–1681
- Trager, S. C., Worthey, G., Faber, S. M., Burstein, D., & Gonzalez, J. J. 1998, ApJS, 116, 1
- Zanichelli, A., Garilli, B., Scoddeggio, M., et al. 2005, PASP, 117, 1271